

Tissue and electrode capacitance reduce neural activation volumes during deep brain stimulation

Christopher R. Butson, Cameron C. McIntyre*

Department of Biomedical Engineering, Cleveland Clinic Foundation, 9500 Euclid Avenue ND20, Cleveland, OH 44195, USA

Accepted 20 June 2005

Abstract

Objective: The growing clinical acceptance of neurostimulation technology has highlighted the need to accurately predict neural activation as a function of stimulation parameters and electrode design. In this study we evaluate the effects of the tissue and electrode capacitance on the volume of tissue activated (VTA) during deep brain stimulation (DBS).

Methods: We use a Fourier finite element method (Fourier FEM) to calculate the potential distribution in the tissue medium as a function of time and space simultaneously for a range of stimulus waveforms. The extracellular voltages are then applied to detailed multi-compartment cable models of myelinated axons to determine neural activation. Neural activation volumes are calculated as a function of the stimulation parameters and magnitude of the capacitive components of the electrode-tissue interface.

Results: Inclusion of either electrode or tissue capacitance reduces the VTA compared to electrostatic simulations in a manner dependent on the capacitance magnitude and the stimulation parameters (amplitude and pulse width). Electrostatic simulations with typical DBS parameter settings (-3 V or -3 mA, 90 μ s, 130 Hz) overestimate the VTA by $\sim 20\%$ for voltage- or current-controlled stimulation. In addition, strength-duration time constants decrease and more closely match clinical measurements when explicitly accounting for the effects of voltage-controlled stimulation.

Conclusions: Attempts to quantify the VTA from clinical neurostimulation devices should account for the effects of electrode and tissue capacitance.

Significance: DBS has rapidly emerged as an effective treatment for movement disorders; however, little is known about the VTA during therapeutic stimulation. In addition, the influence of tissue and electrode capacitance has been largely ignored in previous models of neural stimulation. The results and methodology of this study provide the foundation for the quantitative analysis of the VTA during clinical neurostimulation.

© 2005 International Federation of Clinical Neurophysiology. Published by Elsevier Ireland Ltd. All rights reserved.

Keywords: Electrostatic; Quasistatic; Voltage-controlled stimulation; Current-controlled stimulation; Strength-duration relationship

1. Introduction

Electrical stimulation of the nervous system has been used for centuries as a therapeutic treatment for a variety of disorders (Andrews, 2003a,b; Benabid et al., 2000; Hambrecht and Reswick, 1977). The most successful implantable neurostimulation devices have been applied to pain management (spinal cord stimulation (Alo and Holsheimer, 2002; Taylor et al., 2005)), hearing augmentation (cochlear

implants (Rubinstein and Hong, 2003; Tyler et al., 2003)), and movement disorders (deep brain stimulation (McIntyre et al., 2004a; Walter and Vitek, 2004)). Despite these wide ranging clinical successes it remains difficult to measure or predict the effects of stimulation at the neuronal level. As a result, modeling and simulation have played increasingly important roles in the engineering design and scientific analysis of neurostimulation technology.

The theoretical analysis of neural stimulation has generated two fundamental axioms. First, the electric field generated by the stimulation is dependent on the shape of the electrode, the distribution of cathode(s) and anode(s) and the biophysical properties of the tissue medium (Malmivuo and

* Corresponding author. Tel.: +1 216 445 3264; fax: +1 216 444 9198.
E-mail address: mcintyc@ccf.org (C.C. McIntyre).

Plonsey, 1995). Second, the neural response to the applied electric field is related to the second spatial derivative of the extracellular potentials distributed along each neural process (McNeal, 1976; Rattay, 1986; Warman et al., 1992). We have previously developed detailed models of the electric field generated by stimulating electrodes and designed techniques to quantify the neural response to the applied fields (McIntyre and Grill, 2001; McIntyre et al., 2004b). However, the effects of electrode and tissue capacitance are traditionally ignored in models of neurostimulation, where the electrode is represented as a perfect voltage or current source and the surrounding tissue as a purely conductive medium (quasi-static or electrostatic assumption (Malmivuo and Plonsey, 1995; Bedard et al., 2004)). The errors induced by this assumption may be significant in the context of brain stimulation, where ~ 1 mm changes in the spread of activation can have dramatic consequences on therapeutic effects or side effects induced by the stimulation (Volkman et al., 2002). In turn, attempts to quantitatively evaluate the volume of tissue activated (VTA) as a function of the stimulation parameters require models that accurately account for each component of the neurostimulation system.

Neurostimulation devices utilize either current-controlled or voltage-controlled pulse generators. During reversible (non-faradaic) reactions at the electrode-tissue interface, electrode capacitance influences the electric field transmitted to the tissue during voltage-controlled stimulation and conversely tissue capacitance exerts an influence during current-controlled stimulation (see Discussion). These reactive components can affect the shape and amplitude of the stimulus waveform delivered to the tissue medium and can modulate the neural response to the applied electric field. While previously ignored, the capacitive components of the electrode-tissue interface may represent an important factor in estimating the VTA. To address this limitation, we developed an integrated spatiotemporal model of current- or voltage-controlled neurostimulation in the context of deep brain stimulation (DBS) that quantified the activation of axons surrounding the electrode. Myelinated axons represent highly excitable neural elements surrounding extracellular stimulating electrodes and recent clinical, experimental, and theoretical analysis has suggested the therapeutic response to DBS is linked with axonal activation (Hashimoto et al., 2003; Holsheimer et al., 2000b; McIntyre et al., 2004b). The purpose of this study was to determine the role of capacitance on the volume of axonal tissue activated with clinically relevant deep brain stimulation parameters.

2. Methods

This study utilized detailed computer models of neurostimulation that integrate finite-element based electric field solutions and multi-compartment cable models of myelinated axons. The Poisson equation was solved with

the Fourier finite element method (Fourier FEM) to determine the voltage distribution in the tissue medium, which was subsequently interpolated onto the model axons. These axons were used to search for threshold stimulus amplitudes necessary for action potential generation. The fundamental goal of these models was to predict the effects of electrode capacitance and bulk tissue capacitance on neural activation using DBS electrodes in the context of voltage- and current-controlled stimulation.

2.1. Fourier FEM

Axisymmetric finite element models of DBS electrodes were created with variable resolution meshes of 13,201 nodes for monopolar stimulation and 17,229 nodes for bipolar stimulation using FEMLAB 3.1 (COMSOL, Inc., Burlington, MA). The axisymmetric volume conductor measured 10 cm tall by 5 cm wide. The tissue medium was modeled as homogeneous and isotropic with conductivity of 0.3 S/m, a representative value for brain tissue (Ranck, 1963). The electrode geometry was based on the Medtronic 3387/3389 quadripolar DBS electrode (contact dimensions: 1.5 mm height, 1.27 mm diameter). Voltage or current sources were specified at the electrode contact, and the electrode shaft was modeled as an electrical insulator. The Poisson equation was solved using direct matrix inversion (UMFPACK solver) at each component frequency of the stimulus waveform to determine the potential distribution (V_e) generated within the tissue medium (stiffness matrix σ) based on a collection of sources (I):

$$\nabla \cdot \sigma \nabla V_e = -I$$

To mimic the effects of an indifferent return electrode, ground nodes were placed around the exterior boundary of the finite element mesh for monopolar stimulation. During bipolar stimulation a second electrode was added with a 1.5 mm gap between contacts and the ground nodes were removed from the exterior boundary. Dirichlet and von Neumann boundary conditions were imposed to control voltage or current values at the electrode surface and confine current flow to within the finite element model, respectively.

The Fourier FEM provides a technique to calculate time- and space-dependent voltages within bioelectric volume conductors. This is accomplished with four steps for each solution. First, the stimulus waveform to be applied through the electrode contact is constructed in the time domain (Fig. 1A). The stimulus can be any arbitrarily complex waveform, however in this study we concentrate on simple square waves and Medtronic Irel II DBS pulse generator waveforms because of their immediate applicability to clinical neurostimulation. Next, the waveform is converted from the time domain to the frequency domain using a discrete Fourier transform (DFT) in Matlab (Mathworks, Natick, MA) which provides the magnitude and phase of a set of frequency components that make up the time domain

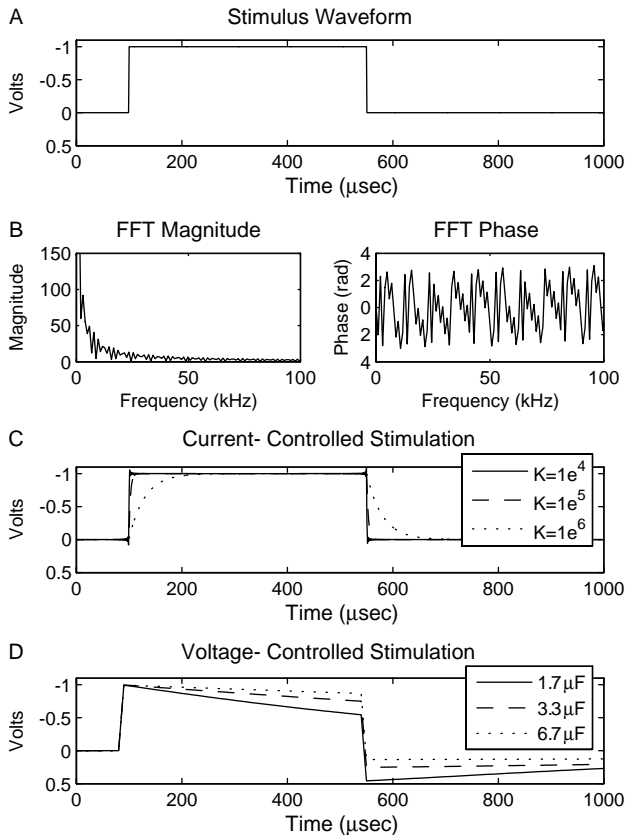


Fig. 1. Fourier FEM method. (A) The stimulus waveform was created in the time domain and (B) subsequently converted to the frequency domain (magnitude and phase shown) using a discrete Fourier transform. The voltage waveform within the volume during (C) current-controlled stimulation and (D) voltage-controlled stimulation was calculated from the Fourier FEM solver. The differences between the original and Fourier FEM waveforms were dependent on pulse width and capacitance values.

stimulus (Fig. 1B). Third, the Poisson equation is solved at each frequency component of the DFT using direct matrix inversion. The standard Poisson equation with purely conductive elements represents an electrostatic solution that does not allow reactive components. To address this limitation we constructed a complex stiffness matrix ($\sigma + i\omega$) that takes into account the capacitive components of the electrode and tissue. The result at each component frequency is scaled and phase shifted according to the results of the DFT. Finally, the resulting waveform is converted back to the time domain with an inverse Fourier transform using Matlab (Fig. 1C and D). Solutions were calculated at 1024 frequencies between 0 and $1/(2*dt)$ Hz, where dt specifies the waveform time step size of 1×10^{-5} s for voltage-controlled stimulation and 1×10^{-6} s for current-controlled stimulation.

A capacitance value of $3.3 \mu\text{F}$ for DBS electrodes was derived from experiments reported by Holsheimer et al. (2000a). This value is also consistent with values predicted by Merrill et al. for polarizable electrodes (Merrill et al., 2005). We also tested half ($1.65 \mu\text{F}$) and twice ($6.66 \mu\text{F}$) this value to characterize the sensitivity of the results on this

parameter. The electrode was treated as purely capacitive with only reversible (non-faradaic) reactions occurring at the electrode-tissue interface. Tissue capacitance values for neural tissue were estimated from previous work (Foster and Schwan, 1989; Schwan and Kay, 1957) with upper and lower bounds for the dielectric constant K between 1×10^4 and 1×10^6 for frequencies below 1 kHz, the frequency limit normally associated with the quasistatic approximation. The relationship between permittivity (ϵ) and dielectric constant is given by:

$$\epsilon = K\epsilon_0$$

where ϵ_0 is the permittivity of free space ($8.85 \times 10^{-12} \text{ C}^2/\text{N m}^2$). Therefore, permittivity values of 8.85×10^{-8} , 8.85×10^{-7} and $8.85 \times 10^{-6} \text{ F/m}$ were employed with corresponding time constants (ϵ/σ) of 0.3×10^{-6} , 3×10^{-6} and 30×10^{-6} s.

2.2. Neural threshold prediction

Field-axon simulations were conducted using Fourier FEM DBS electrode models coupled to $5.7 \mu\text{m}$ diameter myelinated axon models (McIntyre et al., 2002) (Fig. 2A). A collection of 119 model axons were distributed in a 17×7 matrix oriented perpendicular to the electrode shaft. This orientation of axons was used to identify the spatial extent of activation in the vertical and horizontal directions relative to the electrode shaft (localization of activation in axons oriented parallel to the shaft would be ambiguous in the vertical direction). The axons were placed from 1 mm to 4 mm lateral to the electrode and from +4 mm above to -4 mm below the center of the electrode contact (Fig. 2B). The four axons labeled with a 'C' were used to evaluate strength-duration time constants. Each model axon included 21 nodes of Ranvier with 0.5 mm internodal spacing. Voltage values from the Fourier FEM solution were interpolated onto the length of the cable model, and the time-dependent transmembrane potential variations induced by the stimulation were calculated in NEURON v5.7 (Hines and Carnevale, 1997). A range of square wave pulse widths from 60 to $450 \mu\text{s}$ were used in the simulations, corresponding to the range available from the Medtronic DBS pulse generator. At each axon and for each stimulus waveform, threshold stimulus amplitudes were defined that generated action potentials in a one-to-one ratio with the stimulus frequency. The threshold values were used to create 2D contours to define the boundary of activation as a function of the stimulus amplitude. These contours were swept around the axis of the electrode to determine the VTA.

2.3. Chronaxie calculation

Strength-duration curves were generated for individual axons using a range of pulse widths from 60 to $450 \mu\text{s}$.

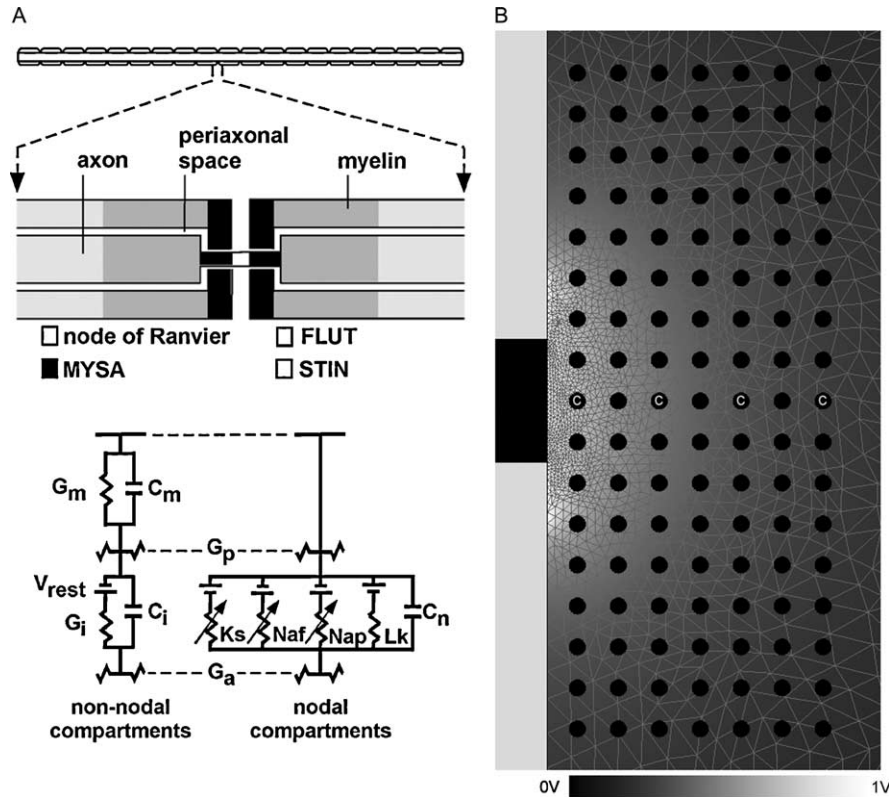


Fig. 2. Cable model axons and finite element model. (A) 5.7 μm diameter myelinated cable model axon for calculation of stimulation thresholds (see McIntyre et al., 2002 for details). Each model axon included 21 nodes of Ranvier with 0.5 mm internodal spacing. Each internodal section of the model consisted of two paranodal myelin attachment segments (MYSA), two paranodal main segments (FLUT), and six internodal segments (STIN). The nodal membrane dynamics included fast (N_{af}) and persistent (N_{ap}) sodium, slow potassium (K_s), and linear leakage (L_k) conductances in parallel with the nodal capacitance (C_n). The internodal segments were represented by a double cable structure of linear conductances with an explicit representation of the myelin sheath (G_m in parallel with C_m) and the internodal axolemma (G_i in parallel with C_i). (B) Axisymmetric FEM model of the electrode and surrounding medium (mesh outline in background). The electrode shaft (left side of picture) was an electrical insulator; the contact (black area of shaft) was a voltage or current source. Tissue medium had a conductivity of 0.3 S/m and dielectric constant from 1×10^4 to 1×10^6 F/m, while the electrode capacitance ranged from 1.66 to 6.65 μF . A 17×7 array of axons was oriented perpendicular to the electrode (black circles, normal to the page) at distances from 1 to 4 mm lateral to the axis of the electrode in 0.5 mm increments, and from -4 to $+4$ mm vertically relative to the center of the electrode in 0.5 mm increments. Axons labeled with a 'C' were used for chronaxial calculation. The voltage solution (background shading according to scale at bottom) within the tissue medium was interpolated onto the cable model axons to determine action potential threshold.

In each case the axon was oriented perpendicular to the electrode shaft at distances of 1, 2, 3 or 4 mm lateral from the axis of the electrode (Fig. 2B, axons labeled 'C'). Chronaxial estimates were determined from the Weiss Equation modified for voltage-controlled stimulation (Holsheimer et al., 2000b):

$$V_{th}PW = V_{th}PW + V_{th}T_{ch}$$

where V_{th} is the threshold voltage, PW is cathodic pulse width, V_{th} is rheobase voltage and T_{ch} is chronaxial. Four experimental conditions were tested: electrostatic model with monophasic waveforms under monopolar stimulation; capacitive electrode model with monophasic waveforms under monopolar stimulation; capacitive electrode model with Medtronic waveforms under monopolar stimulation; capacitive electrode model with Medtronic waveforms under bipolar stimulation. Our modeled Medtronic Irel II waveforms were based on direct measurements from an actual stimulator and are biphasic and charge-balanced with

a cathodic pulse equal to the user defined pulse width followed by an anodic recharge pulse. The anodic pulse begins ~ 0.4 ms after the end of the cathodic pulse and ends ~ 4 ms before the beginning of the next cathodic pulse. The pulse generator voltage was equal to the peak-to-peak voltage between cathodic and anodic phases of the stimulus waveform.

3. Results

The fundamental goals of this study are to quantify the effects of electrode capacitance and bulk tissue capacitance on the volume of tissue activated (VTA) during voltage-controlled and current-controlled DBS. We address the effects of time-dependence of the electric field, stimulation waveform and electrode configuration (monopolar or bipolar) on axonal stimulation thresholds. We also address the influence of electrode capacitance on the strength-duration

relationship generated under voltage-controlled DBS and compare our results to clinical measurements.

3.1. Effects of bulk tissue capacitance on the VTA

Bulk tissue capacitance influences the time-course of the electric field generated in the tissue medium under the context of current-controlled stimulation. The difference in time course between the electrostatic model and the bulk tissue capacitance model causes a difference in the VTA. This difference is a function of the stimulation parameter settings (Fig. 3). During current-controlled stimulation, larger errors occur with shorter pulse widths because the differences between the electrostatic and capacitive waveforms are greatest at the beginning of the cathodic phase (Fig. 3A). The difference between the capacitive and electrostatic models is positively correlated with the dielectric value and stimulus amplitude, and is diminished for longer pulse widths (Fig. 3B). Fig. 3C shows the percent volume error for each pulse width and capacitance value across all current levels. For a comparable DBS stimulation parameter setting such as -3 mA , $90\ \mu\text{s}$,

130 Hz and a dielectric value of 1×10^6 , the electrostatic model overestimates the VTA by $\sim 18\text{ mm}^3$ or $\sim 20\%$. This effect is modulated by the dielectric constant of the tissue medium and the impedance of the volume ($\sim 400\ \Omega$ in this model). Larger dielectric values cause the system to have a longer time constant ($\tau = RC$), which exacerbates the magnitude of the electrostatic error.

3.2. Effects of electrode capacitance on the VTA

Electrode capacitance influences the time-course and amplitude of the stimulus waveform transmitted to the tissue medium under the context of voltage-controlled stimulation. The differences between the stimulus waveforms of the electrostatic and electrode capacitance models result in different VTAs as a function of the stimulation parameters (Fig. 4). During voltage-controlled stimulation, the difference between the capacitive and electrostatic models is inversely proportional to the capacitance value, and is greater for longer pulse widths and larger stimulus amplitudes (Fig. 4B). Fig. 4C shows the percent volume error for each pulse width and capacitance value across all

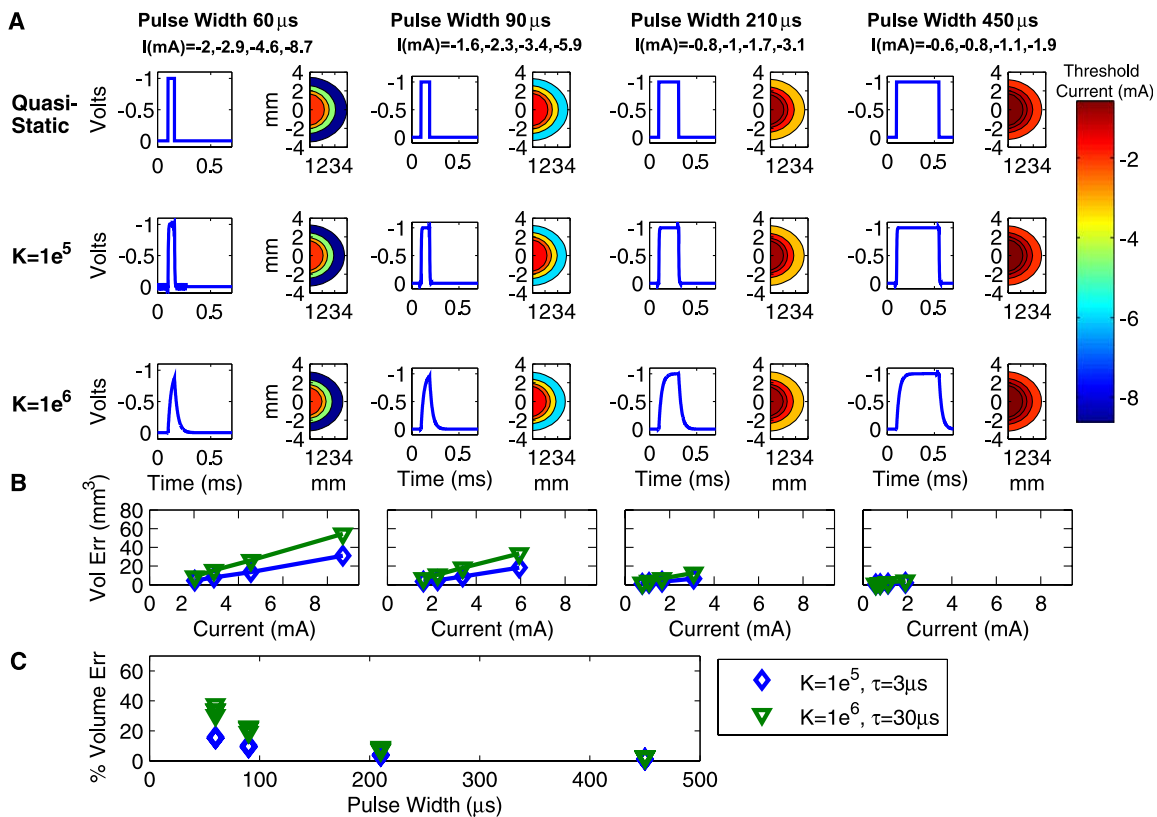


Fig. 3. VTA resulting from current-controlled monopolar stimulation. (A) Results are organized by dielectric values (rows) and pulse width (columns). Within each combination of dielectric and pulse width values are a pair of graphs. The graph on the left shows the time-dependent voltage waveform as calculated by the Fourier FEM solver at one representative point in the volume. The graph on the right is a spatial filled contour plot of the extent of the VTA as determined by threshold amplitude values, which correspond to the scale at right. (B) The volume in cubic millimeter by which the electrostatic model overstates the VTA compared to each dielectric value. Results are displayed as a function of stimulation current, where current values are consistent within each pulse width for the graphs in (A) and (B) as indicated by the column heading labels in (A). (C) Percent by which electrostatic model overstates VTA as a function of pulse width for current-controlled stimulation. Results are shown for different dielectric values with corresponding system time constants. Parts (B) and (C) share the legend.

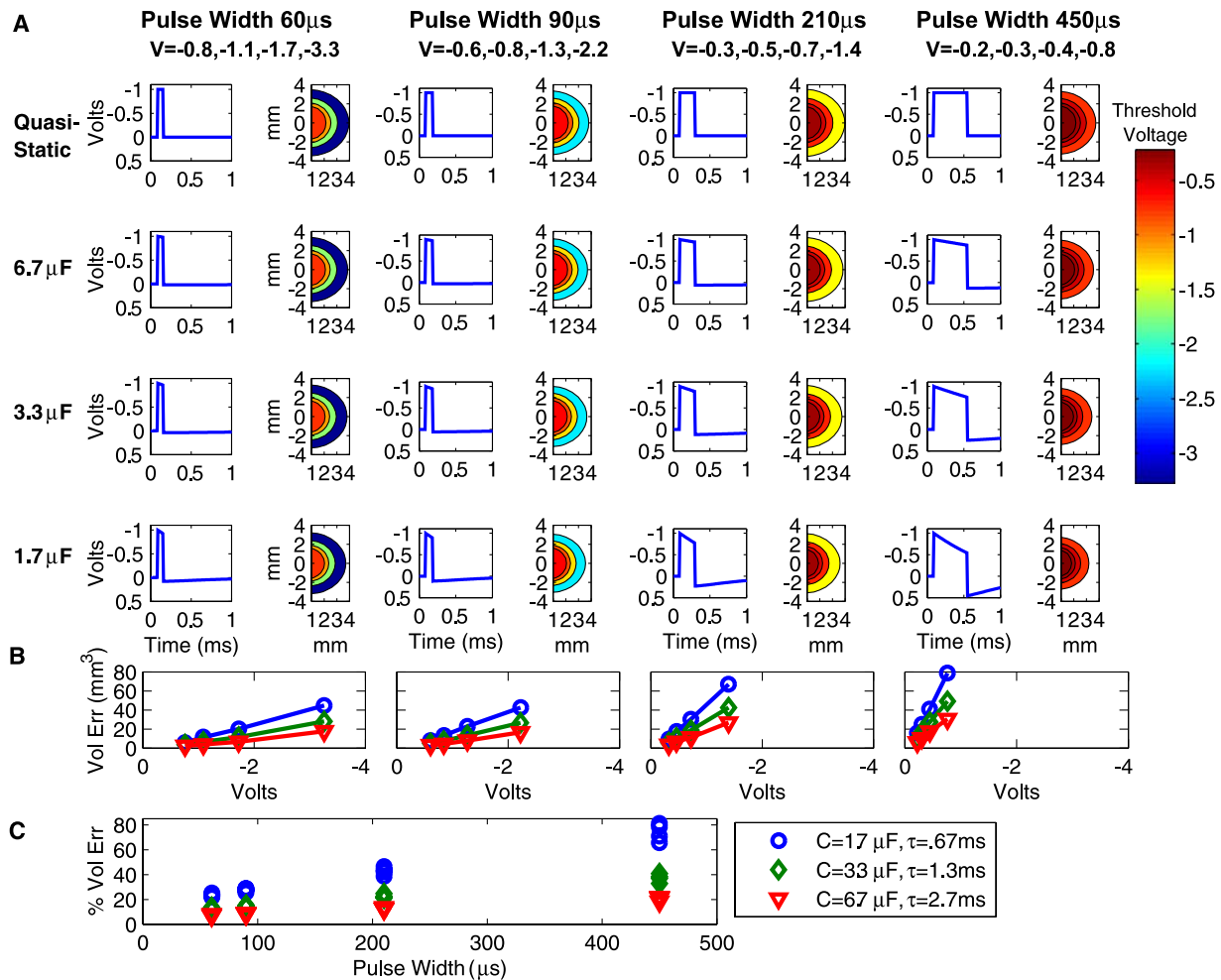


Fig. 4. VTA resulting from voltage-controlled monopolar stimulation. (A) Results are organized by capacitance values (rows) and pulse width (columns). Within each combination of capacitance and pulse width values are a pair of graphs. The graph on the left shows the time-dependent voltage waveform as calculated by the Fourier FEM solver at one representative point in the volume. The graph on the right is a spatial filled contour plot of the extent of the VTA as determined by threshold voltage values, which correspond to the scale at right. (B) The amount in cubic millimeter by which the electrostatic model overstates the VTA compared to each capacitance value. Results are shown as a function of stimulation voltage, where voltage values are consistent within each pulse width for the graphs in (A) and (B) as indicated by the column heading labels in (A). (C) Percent by which electrostatic model overstates VTA as a function of pulse width for voltage-controlled stimulation. Results are shown for different capacitance values with corresponding system time constants. Parts (B) and (C) share the legend.

voltage levels. For a typical DBS stimulation parameter setting such as -3 V, 90μ s, 130 Hz and a standard electrode capacitance value of 3.3μ F, the electrostatic model overestimates the VTA by $\sim 30 \text{ mm}^3$ or $\sim 20\%$. This effect is modulated by the electrode capacitance value and the impedance of the volume ($\sim 400 \Omega$ in this model). Smaller capacitance values cause the system to have a shorter time constant ($\tau = RC$), which exacerbates the magnitude of the electrostatic error.

3.3. Effects of electrode capacitance and stimulation waveform on the strength–duration relationship

Threshold stimulation values, as a function of pulse width, were calculated for axons oriented perpendicular to the electrode shaft under four conditions (Fig. 5A): Case (1)

electrostatic model with monophasic waveforms under monopolar stimulation; Case (2) capacitive electrode model with monophasic waveforms under monopolar stimulation; Case (3) capacitive electrode model with Medtronic waveforms under monopolar stimulation; Case (4) capacitive electrode model with Medtronic waveforms under bipolar stimulation. In our model, a 3 mm electrode-to-axon distance resulted in threshold voltages comparable to those recorded in clinical DBS strength–duration experiments (Ashby et al., 1999; Holsheimer et al., 2000b; Rizzone et al., 2001). However, it should be noted that the impedance of our model ($\sim 400 \Omega$) is lower than the commonly observed clinical measurement of $\sim 1000 \Omega$ (see Discussion). In turn, the VTA for a given stimulus voltage in our model is an overestimation of the VTA generated with higher impedance electrodes. Independent of

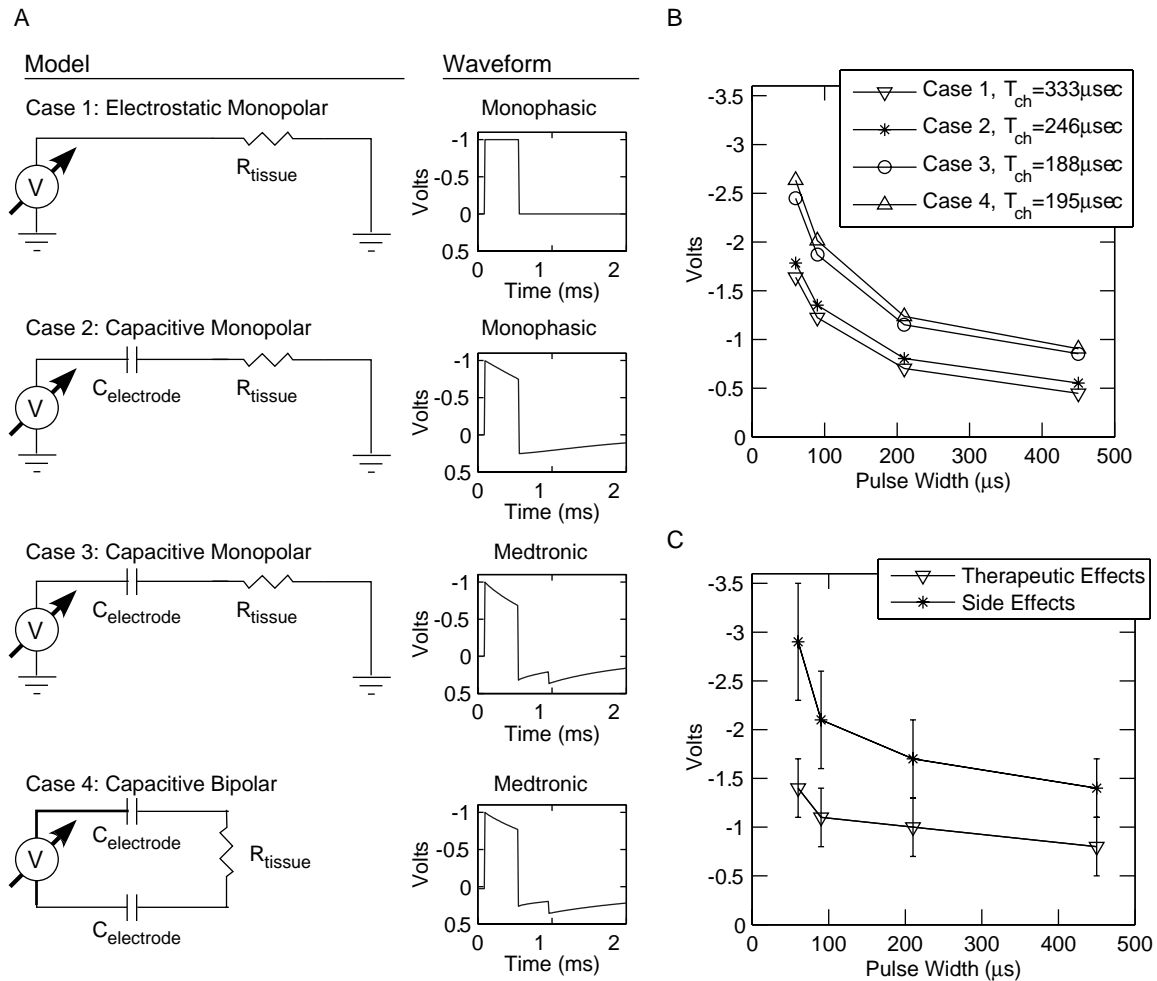


Fig. 5. Dependence of chronaxie values on model and waveform. (A) Threshold voltages were determined for axons located 3 mm lateral from the electrode axis at 130 Hz, 60–450 μ s pulse widths. Four different models were evaluated; a representative circuit diagram and sample waveform is shown for each. (B) Strength–duration curves for the four cases in part A with associated T_{ch} values. Results for cases 1 through 3 reflect monopolar stimulation while Case 4 reflects bipolar stimulation. (C) Strength–duration curves for therapeutic effects and side effects of clinical monopolar DBS settings (\pm standard deviation) from Rizzone et al. (2001).

model impedance, threshold amplitudes progressively increased and T_{ch} progressively decreased from Cases 1 to 3 for an axon stimulated at 130 Hz, while Cases 3 and 4 had comparable results (Fig. 5). These results show that incremental changes in the model realism can generate measurable changes in model output. In addition, experimental estimates of T_{ch} (\sim 100 μ s) from DBS patients (Holsheimer et al., 2000a,b; Rizzone et al., 2001), match most closely with our more realistic DBS models.

Chronaxie values were also dependent on electrode-to-axon distance, stimulus waveform, and stimulation frequency. The T_{ch} of axons 1, 2, 3, and 4 mm lateral from the electrode axis were 238, 296, 333 and 356 μ s, respectively, for 130 Hz stimulation under Case 2. We also compared chronaxie values between Cases 2, 3 and 4 at 100 Hz (the lowest recommended frequency for clinical DBS for movement disorders), 130 Hz (common frequency for clinical DBS) and 185 Hz (the maximum frequency

for the Medtronic pulse generator). Results are summarized in Table 1 for axons located 3 mm from the electrode axis and show that T_{ch} is dependent on both stimulus waveform and frequency. The Medtronic waveform generated a decreasing T_{ch} with increasing stimulation frequency, while the monophasic waveform exhibited a slight increase in T_{ch} over the same frequency range.

Table 1
DBS chronaxie values

Waveform	Configuration	T_{ch} (μ s), 100 Hz	T_{ch} (μ s), 130 Hz	T_{ch} (μ s), 185 Hz
Monophasic	Monopolar	235	246	262
Medtronic	Monopolar	204	188	144
Medtronic	Bipolar	214	195	126

Chronaxie values calculated for a 5.7 μ m diameter myelinated axon oriented perpendicular to the electrode shaft, 3 mm lateral from the axis of the electrode, using voltage-controlled electric field models with an electrode capacitance of 3.3 μ F.

4. Discussion

The results of this study provide three important considerations for the theoretical analysis of the effects of clinical neurostimulation. First, explicit representation of electrode capacitance is important for accurate estimation of the VTA generated by voltage-controlled stimulation. Second, explicit representation of the bulk tissue capacitance can be important for accurate estimation of the VTA generated by current-controlled stimulation, depending on the dielectric constant of the tissue medium. Third, DBS strength–duration time constants are dependent on capacitive components of the electrode-tissue interface and the actual Medtronic stimulation waveform (versus a simple monophasic waveform). We concentrated our analysis on DBS technology, but the results and methodology of this study are applicable to the field of neurostimulation in general.

4.1. Electrical model of the electrode-tissue interface

Electrical circuit models of the electrode-tissue interface typically include the double-layer capacitance (C_{dl}) of the electrode in parallel with a lumped non-linear complex

impedance ($Z_{Faradaic}$) (Gimsa et al., 2005; Holsheimer et al., 2000a; Merrill et al., 2005). $Z_{Faradaic}$ becomes activated when the stimulation exceeds the charge carrying capacity of the C_{dl} . In our simulations we assume that the electrode can be modeled as a pure capacitor. With this assumption we can represent the source, electrode and tissue medium with a set of simplified circuit diagrams as shown in Fig. 6A. We assume that the electrode contact is perfectly polarizable, and that only non-faradaic (reversible) reactions are occurring at the electrode-tissue interface (Merrill et al., 2005). The charge storage capacity of platinum-iridium electrodes (as used in DBS) is $\sim 100 \mu\text{C}/\text{cm}^2$, sufficiently exceeding the $30 \mu\text{C}/\text{cm}^2$ limit employed in clinical neurostimulation (Brunner and Turner, 1977; Rose and Robblee, 1990). We also assume that the neural tissue medium can be crudely represented with bulk capacitance and conductivity values (Bedard et al., 2004).

This set of assumptions limits the effects of the capacitive components to specific stimulation types. The tissue capacitance will only exert an influence during constant current stimulation because the electrode and tissue components behave as independent circuits. Independent of the stimulus waveform, all of the stimulus current will pass through the tissue and hence the electrode capacitance can

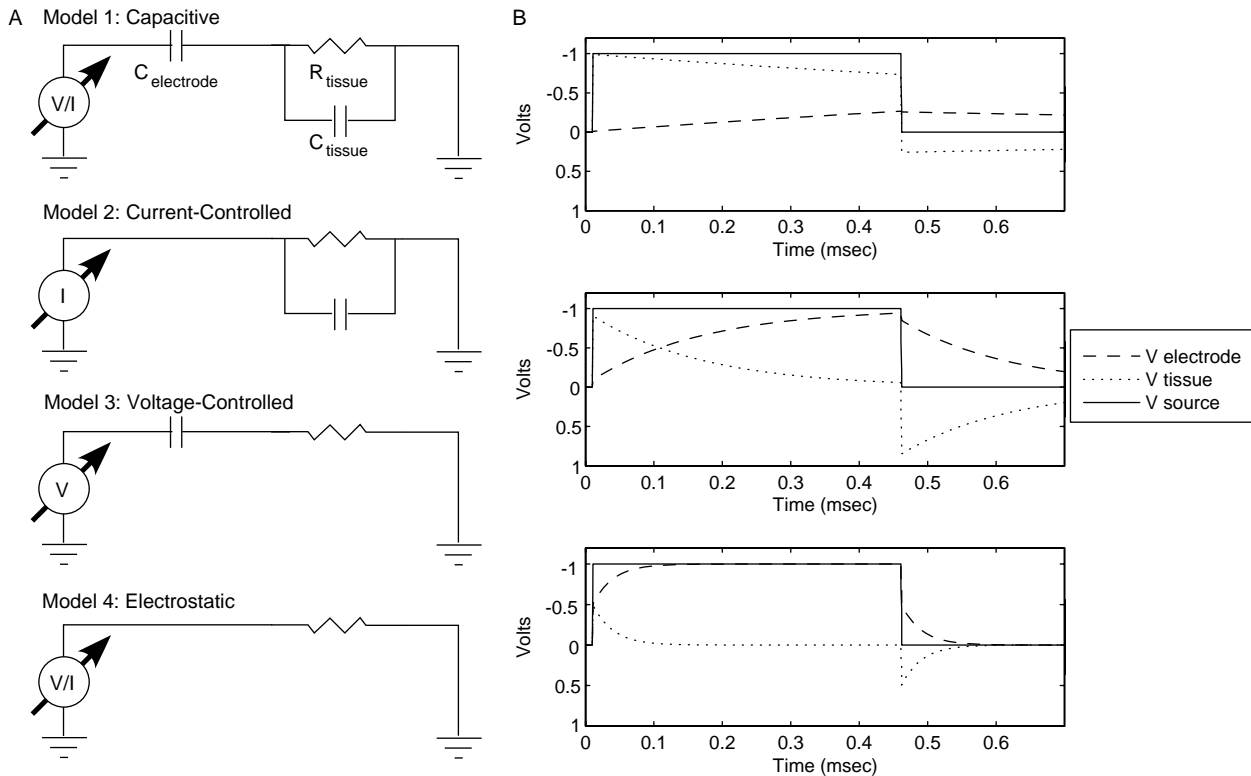


Fig. 6. Equivalent circuit diagrams of neural stimulation field model. (A) Model 1: neural stimulation system including voltage or current source, electrode capacitance, tissue resistance and tissue capacitance. Model 2: Under current-controlled stimulation the electrode capacitance can be ignored. Model 3: Under voltage-controlled stimulation with DBS electrodes the tissue capacitance can be ignored. Model 4: Electrostatic approximation which includes only tissue resistance. (B) Interaction between electrode and tissue capacitance may occur during voltage-controlled stimulation when their values are comparable. Three cases are shown, each of which details the response of the full circuit model from part (A) under voltage-controlled stimulation for varying $C_{electrode}/C_{tissue}$ ratios. Case 1: For the DBS electrode the interactions between electrode and tissue capacitance causes an error of about 1% in V_{tissue} , $\tau = 1.3$ ms. Case 2: For a $C_{electrode}/C_{tissue}$ ratio of 10, V_{tissue} is reduced by 10%, $\tau = 163 \mu\text{s}$. Case 3: A $C_{electrode}/C_{tissue}$ ratio of 1 causes a 50% reduction in V_{tissue} and reduces τ to 28.7 μs .

be ignored. The only complicating issue is that $C_{\text{electrode}}$ has nowhere to discharge and will experience voltage increases during each pulse. However, the monophasic waveforms used in this study are rarely used in practice because they are known to cause tissue damage. Charge-balanced, biphasic waveforms are used in therapeutic devices and these serve to discharge $C_{\text{electrode}}$ during each waveform cycle. Alternately, the effects of the tissue capacitance can be ignored during voltage-controlled stimulation because capacitance of the DBS electrode is about two orders of magnitude greater than the tissue capacitance. As a result, during voltage-controlled stimulation the voltage change across the neural tissue capacitance is much smaller than across the electrode capacitance.

However, a question naturally arises: do the effects of electrode and tissue capacitance interact? If so, under what conditions? Since tissue capacitance values are a property of the neural medium they are unlikely to change substantially in different experimental conditions. Electrode capacitance, on the other hand, is a function of the electrode material and size. Electrodes with limited charge carrying capacity and/or small size may reduce the electrode capacitance to a point where interaction between both tissue and electrode capacitances may affect the stimulus waveform transmitted to the tissue. Greater VTA errors result from smaller capacitance values and smaller electrode time constants (Fig. 4). At the onset of the stimulus pulse both the electrode and tissue capacitors are discharged and the voltage changes at the rate dV/dt (Fig. 6B) (the tissue resistance is momentarily ignored). The equivalent capacitance of the system for two capacitors in series is given by

$$C_{\text{eq}} = (C1 \times C2)/(C1 + C2)$$

and the current is given by

$$i(t) = C_{\text{eq}} dV/dt$$

From these equations we see that the total current is limited by the rise time of the voltage, which is infinite in theory but finite-valued in model experiments (due to non-zero dt values) and in actual DBS pulse generators. We can now calculate the voltage across each capacitor from

$$V(t) \frac{1}{C} \int i(t) dt$$

This equation demonstrates that the voltage across each capacitor at the end of the stimulus onset is inversely proportional to its capacitance value. Therefore, the electrode and tissue capacitors act as an effective voltage divider, reducing the maximum amplitude of the stimulus applied to the tissue. This will further exacerbate the differences between the electrostatic and Fourier FEM models. For DBS electrodes this effect causes a difference of roughly 1% in the amplitude of the tissue voltage waveform. An electrode one-tenth of the size of the DBS electrode would result in a 10% amplitude reduction, and a 50%

amplitude reduction for an electrode one-hundredth of the size (Fig. 6B).

4.2. Model limitations

In addition to our simplified circuit representation of the electrode–tissue interface, the models utilized in this study have a variety of limitations that should be noted. First, the Fourier FEM solves for steady state solutions and does not model transients. This is not a major issue as it simply assumes that the electrode has been active for several waveform periods, which is normally consistent with therapeutic neurostimulation. Second, the accuracy of the Fourier FEM solver is critically dependent on proper selection of frequency range and resolution. The frequency range is dependent on the time-domain waveform step size (dt) which generally must be one order of magnitude smaller than the fastest time constant in the model. The frequency resolution is dependent on the number of frequencies used in the DFT and must be chosen such that any artificial DC offset is removed. Third, the quantitative accuracy of the stimulation thresholds predicted by the myelinated axon model is presently unclear. The myelinated axon model is highly detailed and able to reproduce a wide range of experimentally measured excitation characteristics (McIntyre et al., 2002), and the underlying physiology of the VTA is based on the concept that the primary targets of DBS are myelinated fibers (Holsheimer et al., 2000b). However, the experimental data presently available only allows for qualitative validation of neural thresholds as a function of extracellular stimulation parameters. Fourth, we did not include the capacitance of the return electrode during monopolar voltage-controlled stimulation. In the case of DBS, the return electrode is the metal casing of the implanted pulse generator with a surface area is several orders of magnitude larger than the stimulating electrode. The large surface area of the return electrode results in a capacitance so large that it has a negligible effect on the field solution and the VTA.

The final major limitation of this study was the representation of the tissue medium. Our volume conductor model ignored the inhomogeneities and anisotropies that exist in neural tissue surrounding DBS electrodes (McIntyre et al., 2004c). The modeled uniform conductivity of 0.3 S/m created an impedance of $\sim 400 \Omega$ during monopolar stimulation and $\sim 650 \Omega$ during bipolar stimulation. These values, calculated by integrating the current flowing through the cathode surface for a 1 V stimulus, ignore the series resistance of the electrode lead wires ($\sim 100 \Omega$) and are representative of the lower end of clinically measured impedances from DBS electrodes (Obeso et al., 2001). Most of the voltage drop occurs within a couple millimeters of the active electrode contacts, and the existence of a low conductivity (encapsulation) layer around the electrode can have a significant effect on impedance and spread of the VTA for a given stimulus

voltage (unpublished observations). Larger model impedance values may better match values seen in human DBS patients ($\sim 1000 \Omega$), but reflect a complex interaction between connectors, electrode surface area, encapsulation, tissue inhomogeneity, and tissue anisotropy which are beyond the scope of this particular study. To isolate the effects of tissue and electrode capacitance on the neural response to stimulation we did not include any type of encapsulation layer around the cathode or anode.

While important limitations remain in our models, the results support the need to critically examine one of the fundamental simplifying assumptions of bioelectric field modeling. The quasistatic (electrostatic) approximation has been used in the neural and cardiac stimulation modeling communities for decades. Traditionally, bioelectric field models have not been intended for explicit quantitative comparisons with experimental or clinical data but instead provide a theoretical testing ground for generalized hypotheses. However, computational and experimental advances have enabled bioelectric field models to become increasingly sophisticated with realistic geometries and more detailed biophysical properties. As a result, bioelectric field modeling has progressed to the point where reactive components of the electrode-tissue interface represent non-negligible factors in VTA estimation.

The estimates of VTA error in electrostatic models predicted in this study depend strongly on capacitance values. While electrode capacitance of clinical neurostimulation devices can be measured with relative ease, values for the bulk capacitance of brain tissue are more difficult to accurately estimate. The effects of tissue capacitance on VTA error can be trivial with K values of 1×10^4 or less. However, it is presently unclear what value best represents brain tissue, or how well it can be approximated with a bulk capacitance value (Bedard et al., 2004). More testing is needed to better estimate tissue properties at frequencies below 1 kHz.

4.3. Implications for modeling of clinical neurostimulation

Detailed computer modeling techniques have recently been employed to gain insight into the fundamental mechanisms of electrical stimulation of the central nervous system (McIntyre and Grill, 1999, 2002; McIntyre et al., 2004b; Rattay, 1998). In addition, limitations in our understanding of the therapeutic mechanisms of DBS have prompted interest in using neurostimulation modeling to estimate the VTA during therapeutic and non-therapeutic stimulation (Butson et al., 2004; McIntyre et al., 2004b,c). The goal is to use this information to develop correlations between activation of anatomical nuclei and either therapeutic outcomes or side effects of the stimulation.

Clinical neurostimulation pulse generators utilize either voltage-controlled or current-controlled stimulation. In either case, capacitance modulates the time dependent

properties of the stimulus waveform transmitted to the tissue medium. Failure to represent these reactive components in neurostimulation models can cause significant errors in VTA calculations (Figs. 3 and 4). This is particularly relevant during DBS, where an error of $\sim 30 \text{ mm}^3$ (over-estimation with quasistatic assumption and typical therapeutic stimulation parameters) could account for $\sim 15\%$ of a target volume such as the subthalamic nucleus (Hardman et al., 2002).

The results of this study cannot be directly correlated with clinical strength–duration DBS experiments because it is presently unclear how the neural response to the stimulation is related to behavioral output (Miocinovic and Grill, 2004). However, a variety of interesting qualitative comparisons can be made between our results and clinical records that only become evident with models that explicitly account for the actual stimulus waveform and electrode capacitance effects of voltage-controlled stimulation. For example, calculation of T_{ch} for axonal stimulation best matches clinical results with our most detailed models (Fig. 5; Holsheimer et al., 2000a,b; Rizzone et al., 2001). In addition, including the Medtronic waveform in the model caused decreasing thresholds and decreasing T_{ch} with increasing stimulus frequency, phenomenon also recorded experimentally (Table 1) (O’Suilleabhain et al., 2003; Rizzone et al., 2001). These results highlight the importance of incorporating details that have previously been ignored in neurostimulation modeling, such as capacitance of the electrode–tissue interface and actual stimulus waveforms generated by clinical devices.

In summary, the results of this study show that use of the quasistatic (electrostatic) assumption can cause significant errors in estimating neural activation during current- or voltage-controlled stimulation. The differential effects between voltage- and current-controlled stimulation are dictated by electrode capacitance and tissue capacitance, respectively. The errors induced by ignoring the capacitance of the electrode–tissue interface are a function of the stimulus waveform, stimulus amplitude and magnitude of the reactive components. In turn, development of realistic estimates of the VTA from clinical neurostimulation devices should incorporate bioelectric field models that account for the electrode and/or bulk tissue capacitance.

Acknowledgements

This work was supported by grants from the American Parkinson Disease Association, the Ohio Biomedical Research and Technology Transfer Partnership, and the National Institutes of Health (NS-50449 & NS-52042). The authors would also like to thank Scott E. Cooper, J. Thomas Mortimer, Michael A. Moffitt, and Dominique M. Durand for helpful discussion on this project.

References

- Alo KM, Holsheimer J. New trends in neuromodulation for the management of neuropathic pain. *Neurosurgery* 2002;50:690–703.
- Andrews RJ. Neuroprotection trek—the next generation: neuromodulation. I. Techniques—deep brain stimulation, vagus nerve stimulation, and transcranial magnetic stimulation. *Ann NY Acad Sci* 2003a;993:1–13.
- Andrews RJ. Neuroprotection trek—the next generation: neuromodulation. II. Applications—epilepsy, nerve regeneration, neurotrophins. *Ann NY Acad Sci* 2003b;993:14–24.
- Ashby P, Kim YJ, Kumar R, Lang AE, Lozano AM. Neurophysiological effects of stimulation through electrodes in the human subthalamic nucleus. *Brain* 1999;122:1919–31.
- Bedard C, Kroger H, Destexhe A. Modeling extracellular field potentials and the frequency-filtering properties of extracellular space. *Biophys J* 2004;86:1829–42.
- Benabid AL, Koudsie A, Pollak P, Kahane P, Chabardes S, Hirsch E, Marescaux C, Benazzouz A. Future prospects of brain stimulation. *Neurol Res* 2000;22:237–46.
- Brunner SB, Turner MJ. Electrical stimulation with Pt electrodes: II—estimation of maximum surface redox (theoretical non-gassing) limits. *IEEE Trans Biomed Eng* 1977;24:440–3.
- Butson CR, Henderson JM, McIntyre CC. Patient-specific models of deep brain stimulation: 3D visualization of anatomy, electrode and volume of activation as a function of the stimulation parameters. *Society for Neuroscience Abstract*; 2004.
- Foster KR, Schwan HP. Dielectric properties of tissues and biological materials: a critical review. *Crit Rev Biomed Eng* 1989;17:25–104.
- Gimsa J, Habel B, Schreiber U, Rienen U, Strauss U, Gimsa U. Choosing electrodes for deep brain stimulation experiments—electrochemical considerations. *J Neurosci Methods* 2005;142:251–65.
- Hambrecht FT, Reswick JB. Functional electrical simulation: applications in neural prostheses. *New York: M. Dekker*; 1977.
- Hardman CD, Henderson JM, Finkelstein DI, Horne MK, Paxinos G, Halliday GM. Comparison of the basal ganglia in rats, marmosets, macaques, baboons, and humans: volume and neuronal number for the output, internal relay, and striatal modulating nuclei. *J Comp Neurol* 2002;445:238–55.
- Hashimoto T, Elder CM, Okun MS, Patrick SK, Vitek JL. Stimulation of the subthalamic nucleus changes the firing pattern of pallidal neurons. *J Neurosci* 2003;23:1916–23.
- Hines ML, Carnevale NT. The neuron simulation environment. *Neural Comput* 1997;9:1179–209.
- Holsheimer J, Dijkstra EA, Demeulemeester H, Nuttin B. Chronaxie calculated from current–duration and voltage–duration data. *J Neurosci Methods* 2000a;97:45–50.
- Holsheimer J, Demeulemeester H, Nuttin B, de Sutter P. Identification of the target neuronal elements in electrical deep brain stimulation. *Eur J Neurosci* 2000b;12:4573–7.
- Malmivuo J, Plonsey R. *Bioelectromagnetism: principles and applications of bioelectric and biomagnetic fields*. New York: Oxford University Press; 1995.
- McIntyre C, Grill W. Excitation of central nervous system neurons by nonuniform electric fields. *Biophys J* 1999;76:878–88.
- McIntyre CC, Grill WM. Finite element analysis of the current-density and electric field generated by metal microelectrodes. *Ann Biomed Eng* 2001;29:227–35.
- McIntyre CC, Grill WM. Extracellular stimulation of central neurons: influence of stimulus waveform and frequency on neuronal output. *J Neurophysiol* 2002;88:1592–604.
- McIntyre CC, Richardson AG, Grill WM. Modeling the excitability of mammalian nerve fibers: influence of after potentials on the recovery cycle. *J Neurophysiol* 2002;87:995–1006.
- McIntyre CC, Savasta M, Walter BL, Vitek JL. How does deep brain stimulation work? Present understanding and future questions *J Clin Neurophysiol* 2004a;21:40–50.
- McIntyre CC, Grill WM, Sherman DL, Thakor NV. Cellular effects of deep brain stimulation: model-based analysis of activation and inhibition. *J Neurophysiol* 2004b;91:1457–69.
- McIntyre CC, Mori S, Sherman DL, Thakor NV, Vitek JL. Electric field and stimulating influence generated by deep brain stimulation of the subthalamic nucleus. *Clin Neurophysiol* 2004c;115:589–95.
- McNeal DR. Analysis of a model for excitation of myelinated nerve. *IEEE Trans Biomed Eng* 1976;23:329–37.
- Merrill DR, Bikson M, Jefferys JG. Electrical stimulation of excitable tissue: design of efficacious and safe protocols. *J Neurosci Methods* 2005;141:171–98.
- Miocinovic S, Grill WM. Sensitivity of temporal excitation properties to the neuronal element activated by extracellular stimulation. *J Neurosci Methods* 2004;132:91–9.
- Obeso JA, Olanow CW, Rodriguez-Oroz MC, Krack P, Kumar R, Lang AE. Deep-brain stimulation of the subthalamic nucleus or the pars interna of the globus pallidus in Parkinson's disease. *N Engl J Med* 2001;345:956–63.
- O'Suilleabhain PE, Frawley W, Giller C, Dewey Jr RB. Tremor response to polarity, voltage, pulsewidth and frequency of thalamic stimulation. *Neurology* 2003;60:786–90.
- Ranck Jr JB. Specific impedance of rabbit cerebral cortex. *Exp Neurol* 1963;7:144–52.
- Rattay F. Analysis of models for external stimulation of axons. *IEEE Trans Biomed Eng* 1986;33:974–7.
- Rattay F. Analysis of the electrical excitation of CNS neurons. *IEEE Trans Biomed Eng* 1998;45:766–72.
- Rizzone M, Lanotte M, Bergamasco B, Tavella A, Torre E, Faccani G, Melcarne A, Lopiano L. Deep brain stimulation of the subthalamic nucleus in Parkinson's disease: effects of variation in stimulation parameters. *J Neurol Neurosurg Psychiatry* 2001;71:215–9.
- Rose TL, Robblee LS. Electrical stimulation with Pt electrodes. VIII. Electrochemically safe charge injection limits with 0.2 ms pulses. *IEEE Trans Biomed Eng* 1990;37:1118–20.
- Rubinstein JT, Hong R. Signal coding in cochlear implants: exploiting stochastic effects of electrical stimulation. *Ann Otol Rhinol Laryngol Suppl* 2003;191:14–19.
- Schwan HP, Kay CF. The conductivity of living tissues. *Ann NY Acad Sci* 1957;65:1007–13.
- Taylor RS, Van Buyten JP, Buchser E. Spinal cord stimulation for chronic back and leg pain and failed back surgery syndrome: a systematic review and analysis of prognostic factors. *Spine* 2005;30:152–60.
- Tyler RS, Dunn CC, Witt SA, Preece JP. Update on bilateral cochlear implantation. *Curr Opin Otolaryngol Head Neck Surg* 2003;11:388–93.
- Volkman J, Herzog J, Kopper F, Deuschl G. Introduction to the programming of deep brain stimulators. *Mov Disord* 2002;17:S181–S7.
- Walter BL, Vitek JL. Surgical treatment for Parkinson's disease. *Lancet Neurol* 2004;3:719–28.
- Warman EN, Grill WM, Durand D. Modeling the effects of electric fields on nerve fibers: determination of excitation thresholds. *IEEE Trans Biomed Eng* 1992;39:1244–54.